Photoredox Catalysis

International Edition: DOI: 10.1002/anie.201603789
German Edition: DOI: 10.1002/ange.201603789

Structural Design Principle of Small-Molecule Organic Semiconductors for Metal-Free, Visible-Light-Promoted Photocatalysis

*Lei Wang, Wei Huang, Run Li, Dominik Gehrig, Paul W. M. Blom, Katharina Landfester, and Kai A. I. Zhang**

Abstract: *Herein, we report on the structural design principle of small-molecule organic semiconductors as metal-free, pure organic and visible light-active photocatalysts. Two series of electron-donor and acceptor-type organic semiconductor molecules were synthesized to meet crucial requirements, such as 1) absorption range in the visible region, 2) sufficient photoredox potential, and 3) long lifetime of photogenerated excitons. The photocatalytic activity was demonstrated in the intermolecular C–H functionalization of electron-rich heteroaromates with malonate derivatives. A mechanistic study of the light-induced electron transport between the organic photocatalyst, substrate, and the sacrificial agent are described. With their tunable absorption range and defined energy-band structure, the small-molecule organic semiconductors could offer a new class of metal-free and visible light-active photocatalysts for chemical reactions.*

Photocatalysts, which can absorb in the visible region, have attracted much attention in recent years as a sustainable tool for chemical synthesis under mild and environmentally benign conditions.[1] Beside the well-developed organometallic complexes based on transition metals, such as $[Ru(bpy)_3]Cl_2$ and *fac*-$[Ir(ppy)_3]$,[2] or recently reported common-metal-based systems, such as copper-containing photocatalysts,[3] pure organic dyes have been also employed as a metal-free variation of photocatalysts for various reactions.[4] Nevertheless, there are some intrinsic drawbacks associated with these molecular systems, for instance, high cost and toxicity of rare metals, limited availability in nature, and photobleaching, which can be troublesome for catalyst stability and long-term usage. The lack of systematically controllable band structures still remains a large challenge. It is therefore important to develop a new class of metal-free, pure organic photocatalysts with easily tunable absorption ranges, and controllable oxidative and reductive potentials for chemical transformations.

Small-molecule organic semiconductors (SMOSs) have been used in a vast number of photoelectronic applications, such as organic light emitting diodes (OLEDs), organic solar cells (OSCs), and organic thin-film transistors (OTFTs) owing to their unique optical and electronic properties originating from the visible-light-responsive π-conjugated backbone structure.[5] The driving force of organic solar cells is electron (hole) transfer at a donor–acceptor (D–A) interface followed by charge separation. An interesting question is whether the light-generated electron-transfer process, which is the operation principle of organic photovoltaic (OPV) devices can be translated into a photocatalytic system for chemical reactions. Recently, macromolecular semiconducting polymeric systems have been introduced as metal-free and heterogeneous photocatalysts for organic reactions[6] or light-induced hydrogen evolution[7] based on a similar principle. In comparison, only a few examples of the SMOSs were reported as homogeneous visible-light-active photocatalysts.[8] A deeper understanding for the design of this new class of small-molecule-based materials is desirable.

As illustrated in Figure 1a, the light-induced electron transfer in OPVs usually occurs from the electron donor to the separated acceptor organic semiconductor (OC) material. By transferring this process into the photocatalytic process, the photo-generated electron/hole pair of the organic semiconductor could function as the reductive and oxidative species, reacting with either electron-accepting or -donating substrates, respectively, and completing the photoredox cycle (Figure 1b). For both applications, the energetic band positions of the organic semiconductor materials could be controlled by employing various building blocks.[9]

To reach high efficiency in the OPVs, the enhanced charge separation and long exciton lifetime is of great importance. This can be achieved by morphology control of the separated D- and A materials in solid state.[10] For the photocatalytic process, which is usually carried out in liquid phase, the same

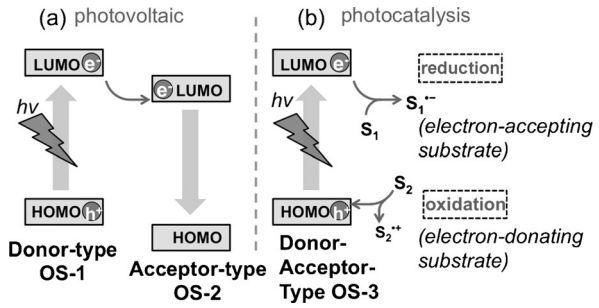

Figure 1. Functional principles of light-induced electron transfer in a) a simplified organic semiconductor (OC)-based photovoltaic device and b) an organic semiconductor-based photocatalytic system. S: substrate.

[*] L. Wang, W. Huang, R. Li, Dr. D. Gehrig, Prof. P. W. M. Blom, Prof. K. Landfester, Dr. K. A. I. Zhang
Max Planck Institute for Polymer Research
55128 Mainz (Germany)
E-mail: kai.zhang@mpip-mainz.mpg.de

Supporting information (experimental details and characterization, scope of the photocatalytic dehalogenation reactions, fluorescence quenching experiments, ^1H and ^{13}C NMR spectra) and the ORCID identification number(s) for the author(s) of this article can be found under http://dx.doi.org/10.1002/anie.201603789.

effect ought to be realized by combining the D and A moieties in a single molecule.

Herein, we report a structural design principle of electron-donor and -acceptor small-molecule organic semiconductors (SMOSs) as a new class of pure organic, metal-free and visible-light-active photocatalytic systems with tunable absorption areas and defined band structures. The oxidative and reductive potentials of SMOSs could be easily controlled by simple variation of the electron-donor and -acceptor moieties in the molecule. The photocatalytic activity was demonstrated in the intermolecular C–H functionalization of electron-rich heteroaromates with malonates under visible light irradiation. It could be observed by mechanistic studies that the light-induced electron transport between the SMOSs, substrates, and the sacrificial electron-donating agent played a significant role in enhancing the photocatalytic efficiency of the SMOSs. Furthermore, the time-resolved photoluminescence spectroscopy demonstrated fluorescence lifetimes of the designed SMOSs ranging from around 12 to 16 ns, indicating long-living photogenerated excitons in the SMOSs.

Two series of electron donor–acceptor type small-molecule organic semiconductors were designed to meet the crucial requirements as organic molecular photocatalysts: 1) absorption range in the visible region, 2) sufficient light-generated redox potential, and 3) long lifetime of the photogenerated excitons. The structures of the SMOSs are displayed in Scheme 1. Containing the same benzothiadiazole (BT) unit as the electron-acceptor moiety, Series 1 represents

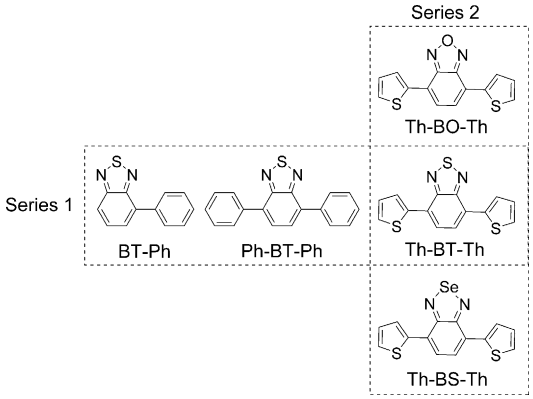

Scheme 1. Structures of the two series of the SMOSs.

different electron-donor variations, such as single phenyl ring (BT-Ph), two phenyl rings (Ph-BT-Ph), and two thiophene units (Th-BT-Th). In comparison, Series 2 shows the opposite structural design principle using thiophene as the electron-donor unit in combination with different benzochalcogenadiazoles, such as benzooxadiazole (Th-BO-Th), benzothiadiazole (Th-BT-Th), and benzoselenadiazole (Th-BS-Th) as the electron acceptor. The synthetic details and characterizations of the SMOSs are described in the Supporting Information.

We chose the intermolecular C–H functionalization of electron-rich heteroaromates with malonates to investigate the photocatalytic activity of the SMOSs. The reaction mechanism could be divided in two half cycles as displayed in Figure 2.[11] The first half reaction is the generation of malonate radical via the reduction of the malonate halide, driven by the transfer of the photo-generated electron from the photocatalyst onto the malonate halide, resulting in the

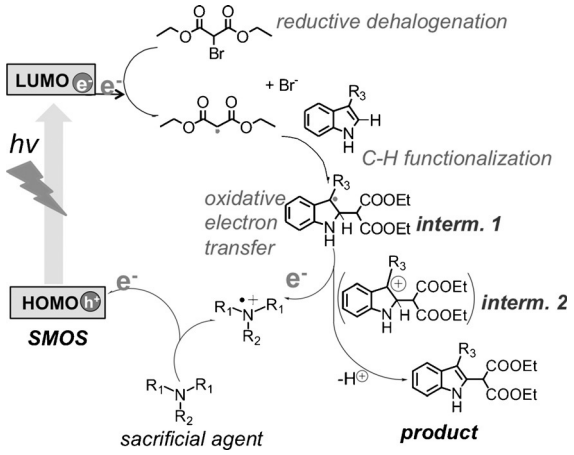

Figure 2. Reaction mechanism of the intermolecular C–H functionalization of electron-rich heteroaromates with diethyl bromomalonates. R_1, R_2, R_3 = aryl or alkyl; interm = intermediate.

malonate radical and halide anion. The malonate radical reacts with the heteroaromates to form the radical intermediate 1. The second half reaction starts first with the oxidation of the sacrificial agent, usually an amine, by the photogenerated hole on the highest occupied molecular orbital (HOMO) level, leading to the formation of cationic radical of the amine and transfer of the extracted electron to the lowest unoccupied molecular (LUMO) level of the catalyst. The full reaction cycle is completed by the electron transfer from the radical intermediate 1 to the oxidized amine radical and the cationic intermediate 2, forming the final product after losing one proton.

To investigate separately the electron transfer from the photocatalyst onto the halide, we conducted first the light-induced dehalogenation reaction of haloketone derivatives using Series 1 as the photocatalysts and diisopropylethylamine (DIPEA) as the electron-donating sacrificial agent (Figure 3a and Table S1 in the Supporting Information). Under the irradiation of a household energy saving light bulb (23 W), Th-BT-Th exhibited the highest reaction rate (Figure 3b), reaching full conversion within 1 h with a low catalyst load (1 mol%), followed by Ph-BT-Ph and BT-Ph. To confirm the proposed electron-transfer pathway as displayed in Figure 3a, we then conducted fluorescence quenching experiments using Series 1 as the photocatalyst (Figure S1–S3). It was shown that the fluorescence of the SMOSs could be gradually quenched by adding DIEPA, while the addition of diethyl bromomalonate did not affect the fluorescence. Another control experiment showed that without using DIEPA, no product was obtained (entry 2, Table S1). This result indicates that for the SMOS-based systems, the excited electron could not be transferred directed to diethyl bromomalonate without employing an electron donor. This further indicates that the electron originated from the sacrificial

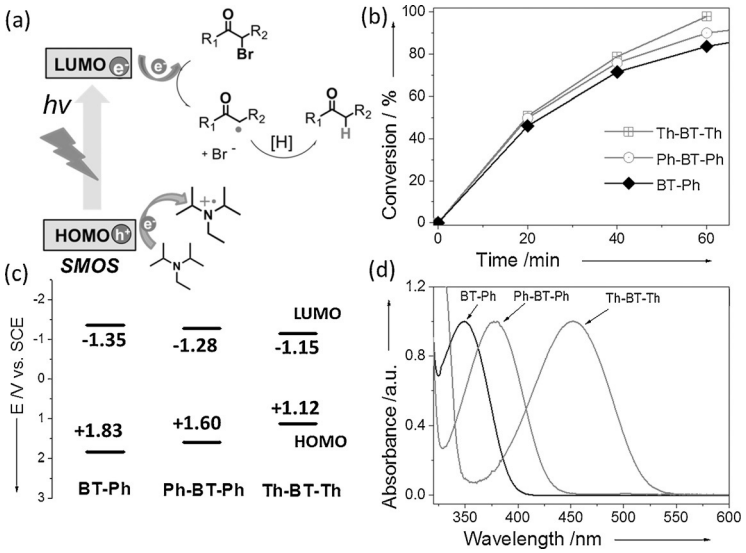

Figure 3. a) Reaction mechanism of light-induced dehalogenation reaction of haloketones using SMOSs as photocatalysts. b) Debromination rates of α-bromoacetophenone as model substrate using Series 1 as catalysts. c) HOMO and LUMO band positions and d) UV/Vis absorption spectra of the SMOSs in Series 1. R_1, R_2 = H, aryl, carboxylate.

agent via oxidative extraction by the photogenerated hole. Similar light-induced electron mediation has been demonstrated by employing polymeric systems as photocatalysts.[6a,b,e,12]

The redox potentials of the SMOSs were derived from the HOMO and LUMO band positions as displayed in Figure 3c. Significantly, the highest oxidative and reductive potentials of Ph-BT (−1.35 V and +1.83 V vs. saturated calomel electrode (SCE)) did not lead to the highest reaction rate within the series. This is because the redox potentials of all three catalysts are sufficient enough for the oxidation of DIPEA (+0.52 V vs. SCE) and for the reduction of α-bromoacetophenone (−0.99 V vs. SCE). The superior catalytic activity of Th-BT-Th should rather attributed to its broader absorption range in the visible region up to 550 nm, while Ph-BT and Ph-BT-Ph mainly absorb in the UV and blue region (Figure 3d). The D–A structure of Th-BT-Th was more advantageous for designing visible light-active photocatalysts.

To complete the reaction cycle of the photocatalytic intermolecular C–H functionalization, we then tested the functionalization reaction of 3-methylindole and diethyl bromomalonate using Series 2 with similar absorption ranges in the visible region (Figure S4). A blue LED lamp (460 nm, 1.2 W cm^{-2}) was used as light source to accelerate the reaction rate. Unlike for the dehalogenation reaction, triphenylamine was used instead of DIPEA to avoid the hydrogen abstraction process by the diethyl malonatyl radical and to increase the final yield.[11] The results are listed in Table 1. It was shown that all three SMOSs could catalyze the reaction in high conversion and yields, with Th-BT-Th again being the most efficient photocatalyst within Series 2 using 3-methylindole as model substrate (entry 2). The superior catalytic efficiency of Th-BT-Th corresponded well with its redox potential, which is sufficient to both reduce diethyl bromomalonate (E_{red} = −1.0 V vs. SCE) and oxidize triphenylamine (E_{oxi} = +0.89 V vs. SCE). In comparison, despite the high oxidation potentials of Th-BO-Th (E_{oxi} = +1.24 V vs. SCE) and Th-BS-Th (E_{oxi} = +1.02 V vs. SCE), their reduction potentials with −1.06 V and −1.08 V (vs. SCE) appeared insufficient to reduce diethyl bromomalonate, indicating that the reductive half cycle might be the rate-determining step. The HOMO/LUMO band positions of the SMOSs and the reduction and oxidation potentials of the substrates and sacrificial agents are displayed in Figure 4a. Additionally, using BT-Ph and Ph-BT-Ph as catalyst lead either to no or a very low yield of product (entry 7 and 8), demonstrating the absorption in the visible range is indispensable. Note that the catalytic efficiency of Th-BT-Th is comparable with the state-of-art photocatalysts based on transition metals, such as $[Ru(bpy)_3]Cl_2$, for the same type of photoredox reactions.[13]

To obtain more insight of the reaction mechanism and to investigate the concrete electron-transfer pathway in the catalytic cycle, we verified the role of the sacrificial agent. It was reported that sacrificial reagents could be replaced by bases to

Table 1: Photocatalytic C–H functionalization of electron-rich heteroaromates with diethyl bromomalonate using the SMOSs as photocatalysts.[a]

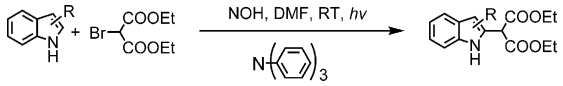

Entry	Catalyst	Substrate	Product	Time [h]	Conv. [%][b]	Yield [%][c]
1	Th-BO-Th		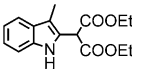	15	>99	82
2	Th-BT-Th		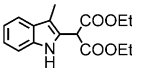	0.75	>99	86
3	Th-BS-Th		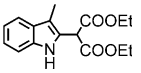	14	>99	85
4	Th-BT-Th		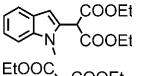	2	>99	78
5	Th-BT-Th	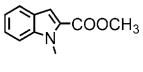	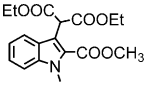	2	>99	87
6	Th-BT-Th		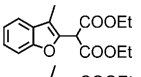	1	>99	90
7	Ph-BT		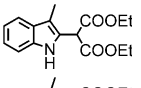	6	0	–
8	Ph-BT-Ph		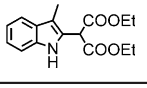	6	20	5

[a] Reaction conditions: 1 equiv (0.38 mmol) heteroarene, 2 equiv diethyl bromomalonate, 2 equiv 4-methoxy-*N*,*N*-diphenylaniline, 1 mol% photocatalyst in 2.5 mL DMF, blue LED (λ = 460 nm).
[b] Determined by GC-MS. [c] Yield of isolated product after purification over SiO_2.

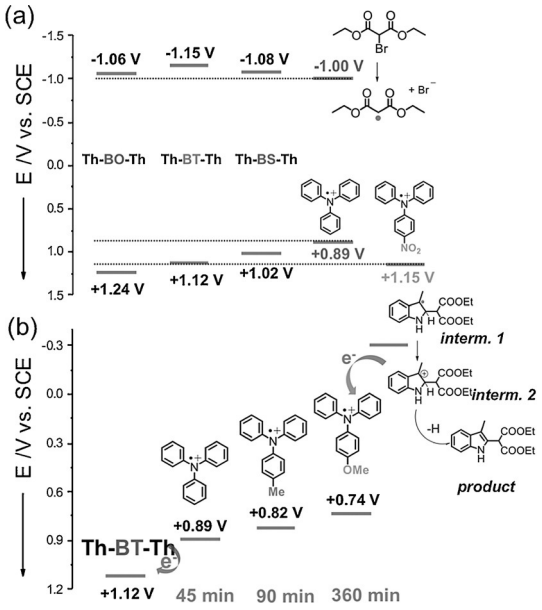

Figure 4. a) HOMO and LUMO band positions of the SMOSs in Series 2 and redox potentials of substrates and sacrificial agents. b) Reaction times with different triphenylamine-based sacrificial agents using Th-BT-Th as the catalyst.

neutralize hydrogen halides formed as side products during the catalytic cycle.[14] However, using K_2HPO_4, $CsCO_3$, K_2CO_3, or $KHCO_3$ as the base for our system did not lead to any consumption of 3-methylindole, confirming the role of the amine not only as a base, but also most likely for mediating the electron transfer from the radical intermediate 1 formed after the C–H functionalization of 3-methylindole with the malonate radical back to the photo-generated hole of the photocatalyst in the full catalytic cycle (Figure 2). To support this idea, we tested 4-nitro-*N*,*N*-diphenylaniline with an oxidative potential of +1.15 V (vs. SCE) as sacrificial agent. By using Th-BT-Th (E_{oxi} = +1.12 V vs. SCE) as photocatalyst, no product could be determined, confirming that the oxidation potential of Th-BT-Th was not sufficient enough to oxidize 4-nitro-*N*,*N*-diphenylaniline, making the electron transfer from the amine to the HOMO level of the catalyst impossible (Figure 4a).

Furthermore, two triphenyl amine derivatives, 4-methyl-*N*,*N*-diphenylaniline (E_{oxi} = +0.82 V vs. SCE) and 4-methoxy-*N*,*N*-diphenylaniline (E_{oxi} = +0.74 V vs. SCE) were employed to manipulate the electron-transfer process from the radial intermediate onto the oxidized amine. As illustrated in Figure 4b, the reaction times of 90 min and 360 min of both amines, respectively, were slower than that of triphenylamine (E_{oxi} = +0.89 V vs. SCE) with 45 min. Similar observations could also be made by employing either Th-BO-Th or Th-BS-Th as the photocatalyst or using different substrates (Figure S5 and S6). This further confirmed the electron-transfer pathway as illustrated in Figure 2 as the main electron-transfer pathway. The other possibility of direct electron transfer from the radical intermediate or eventually from the indole should rather play a minor role within the catalytic cycle. The oxidation potential of the radical intermediate 1 to its oxidized cation intermediate 2 was calculated to be −0.34 V vs. SCE (Figure S12), making the triphenyl amine radical cation the most efficient oxidant with a theoretical overpotential of 1.23 V.

Time-resolved photoluminescence spectroscopy revealed long fluorescence lifetimes for all SMOSs ranging from around 12 to 16 ns, indicating long-living photogenerated excitons for both series (Figure 5a). Furthermore, two tendencies could also be observed: 1) Series 2 with absorption

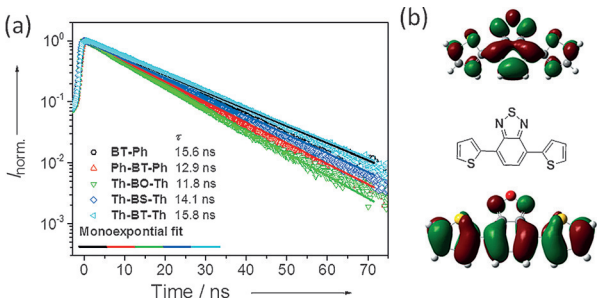

Figure 5. a) Fluorescence-delay spectra of the SMOSs and b) HOMO (bottom) and LUMO (top) of Th-BT-Th calculated at the B3LYP/6-31G* level.

range mainly in the visible region exhibited much higher reaction yields than Series 1 which has absorption mainly in the UV region; 2) Th-BT-Th with the longest fluorescence lifetime of 15.8 ns showed the highest photocatalytic efficiency (Figure S13). Theoretical calculations using the density functional theory (DFT) at B3LYP/6-31G*level showed that the electron densities are mainly focused on the electron-donating thiophene and -withdrawing benzothiadiazole moieties on the HOMO and LUMO for Th-BT-Th (Figure 5b). This clearly demonstrates that the D–A-type molecules could exhibit longer exciton lifetimes, than oligomers based on only donor moieties, such as thiophene, which usually exhibit fluorescence lifetimes shorter than 1 ns.[15] These observations further confirmed that all three parameters, that is, absorption range, sufficient energy band position, and long exciton lifetime are required for highly efficient visible-light-driven catalytic reactions using SMOSs.

In summary, we have developed donor–acceptor (D–A) based small-molecule organic semiconductors (SMOSs) as a new class of pure organic and metal-free photocatalytic systems with tunable absorption range, defined and appropriate energy band positions, and long exciton lifetimes. The photocatalytic activity could be well controlled via variation of the electron-donor and -acceptor combination in the molecular structure. Using the intermolecular C–H functionalization of electron-rich heteroaromates with malonate derivatives as a model reaction, the structural design principle of the SMOSs was demonstrated. The catalytic efficiency of the SMOSs was comparable to that of state-of-art catalysts, such as $[Ru(bpy)_3]Cl_2$. Furthermore, the mechanistic insight of the light-induced electron transport between the organic photocatalyst, substrate, and the sacrificial electron-donating agent confirmed that not only the finely controlled redox potential of the photocatalyst, but also the oxidation potential of the amine-based sacrificial agent could enhance the

catalytic efficiency. With their tunable absorption range, defined and controllable redox potential, long-lived photogenerated excitons, and pure organic nature, the SMOSs could offer a promising class of metal-free and visible light-active photocatalysts for chemical reactions.

Acknowledgements

We thank the Max Planck Society for financial support. L.W., W.H.,and R.L. thank the China Scholarship Council (CSC) for scholarships.

Keywords: C–H functionalization · metal-free catalysts · photocatalysis · small-molecule organic semiconductor · visible light

How to cite: *Angew. Chem. Int. Ed.* **2016**, *55*, 9783–9787
Angew. Chem. **2016**, *128*, 9935–9940

[1] a) D. Ravelli, M. Fagnoni, A. Albini, *Chem. Soc. Rev.* **2013**, *42*, 97–113; b) K. Zeitler, *Angew. Chem. Int. Ed.* **2009**, *48*, 9785–9789; *Angew. Chem.* **2009**, *121*, 9969–9974; c) J. Xuan, W. J. Xiao, *Angew. Chem. Int. Ed.* **2012**, *51*, 6828–6838; *Angew. Chem.* **2012**, *124*, 6934–6944; d) J. M. R. Narayanam, C. R. J. Stephenson, *Chem. Soc. Rev.* **2011**, *40*, 102–113; e) C. K. Prier, D. A. Rankic, D. W. C. MacMillan, *Chem. Rev.* **2013**, *113*, 5322–5363; f) D. A. Nicewicz, D. W. C. MacMillan, *Science* **2008**, *322*, 77–80; g) J. M. R. Narayanam, J. W. Tucker, C. R. J. Stephenson, *J. Am. Chem. Soc.* **2009**, *131*, 8756.

[2] a) S. Ventre, F. R. Petronijevic, D. W. C. MacMillan, *J. Am. Chem. Soc.* **2015**, *137*, 5654–5657; b) J. D. Cuthbertson, D. W. C. MacMillan, *Nature* **2015**, *519*, 74–77; c) E. L. Tyson, M. S. Ament, T. P. Yoon, *J. Org. Chem.* **2013**, *78*, 2046–2050; d) L. R. Espelt, I. S. McPherson, E. M. Wiensch, T. P. Yoon, *J. Am. Chem. Soc.* **2015**, *137*, 2452–2455; e) J. D. Nguyen, E. M. D′Amato, J. M. R. Narayanam, C. R. J. Stephenson, *Nat. Chem.* **2012**, *4*, 854–859; f) C. J. Yao, Q. Sun, N. Rastogi, B. Konig, *ACS Catal.* **2015**, *5*, 2935–2938; g) E. Brachet, T. Ghosh, I. Ghosh, B. Konig, *Chem. Sci.* **2015**, *6*, 987–992; h) R. Brimioulle, D. Lenhart, M. M. Maturi, T. Bach, *Angew. Chem. Int. Ed.* **2015**, *54*, 3872–3890; *Angew. Chem.* **2015**, *127*, 3944–3963.

[3] a) Q. M. Kainz, C. D. Matier, A. Bartoszewicz, S. L. Zultanski, J. C. Peters, G. C. Fu, *Science* **2016**, *351*, 681–684; b) S. Paria, O. Reiser, *ChemCatChem* **2014**, *6*, 2477–2483.

[4] a) S. P. Pitre, C. D. McTiernan, H. Ismaili, J. C. Scaiano, *ACS Catal.* **2014**, *4*, 2530–2535; b) M. Neumann, S. Fuldner, B. Konig, K. Zeitler, *Angew. Chem. Int. Ed.* **2011**, *50*, 951–954; *Angew. Chem.* **2011**, *123*, 981–985; c) K. Ohkubo, K. Mizushima, R. Iwata, K. Souma, N. Suzuki, S. Fukuzumi, *Chem. Commun.* **2010**, *46*, 601–603; d) S. P. Pitre, C. D. McTiernan, H. Ismaili, J. C. Scaiano, *J. Am. Chem. Soc.* **2013**, *135*, 13286–13289; e) K. Ohkubo, T. Kobayashi, S. Fukuzumi, *Angew. Chem. Int. Ed.* **2011**, *50*, 8652–8655; *Angew. Chem.* **2011**, *123*, 8811–8814; f) D. P. Hari, P. Schroll, B. Konig, *J. Am. Chem. Soc.* **2012**, *134*, 2958–2961; g) D. J. Wilger, N. J. Gesmundo, D. A. Nicewicz, *Chem. Sci.* **2013**, *4*, 3160–3165.

[5] a) Y. Lin, Y. Li, X. Zhan, *Chem. Soc. Rev.* **2012**, *41*, 4245–4272; b) A. Mishra, P. Bäuerle, *Angew. Chem. Int. Ed.* **2012**, *51*, 2020–2067; *Angew. Chem.* **2012**, *124*, 2060–2109.

[6] a) F. Su, S. C. Mathew, G. Lipner, X. Fu, M. Antonietti, S. Blechert, X. Wang, *J. Am. Chem. Soc.* **2010**, *132*, 16299–16301; b) F. Su, S. C. Mathew, L. Möhlmann, M. Antonietti, X. Wang, S. Blechert, *Angew. Chem. Int. Ed.* **2011**, *50*, 657–660; *Angew. Chem.* **2011**, *123*, 683–686; c) X. Wang, S. Blechert, M. Antonietti, *ACS Catal.* **2012**, *2*, 1596–1606; d) F. Vilela, K. Zhang, M. Antonietti, *Energy Environ. Sci.* **2012**, *5*, 7819–7832; e) K. Zhang, D. Kopetzki, P. H. Seeberger, M. Antonietti, F. Vilela, *Angew. Chem. Int. Ed.* **2013**, *52*, 1432–1436; *Angew. Chem.* **2013**, *125*, 1472–1476; f) N. Kang, J. H. Park, K. C. Ko, J. Chun, E. Kim, H. W. Shin, S. M. Lee, H. J. Kim, T. K. Ahn, J. Y. Lee, S. U. Son, *Angew. Chem. Int. Ed.* **2013**, *52*, 6228–6232; *Angew. Chem.* **2013**, *125*, 6348–6352; g) K. Zhang, Z. Vobecka, K. Tauer, M. Antonietti, F. Vilela, *Chem. Commun.* **2013**, *49*, 11158–11160; h) S. Ghasimi, S. Prescher, Z. J. Wang, K. Landfester, J. Yuan, K. A. I. Zhang, *Angew. Chem. Int. Ed.* **2015**, *54*, 14549–14553; *Angew. Chem.* **2015**, *127*, 14757–14761; i) M. Baar, S. Blechert, *Chem. Eur. J.* **2015**, *21*, 526–530.

[7] a) X. Wang, K. Maeda, A. Thomas, K. Takanabe, G. Xin, J. M. Carlsson, K. Domen, M. Antonietti, *Nat. Mater.* **2009**, *8*, 76–80; b) J. Zhang, G. Zhang, X. Chen, S. Lin, L. Mohlmann, G. Dolega, G. Lipner, M. Antonietti, S. Blechert, X. Wang, *Angew. Chem. Int. Ed.* **2012**, *51*, 3183–3187; *Angew. Chem.* **2012**, *124*, 3237–3241; c) Y. Wang, X. Wang, M. Antonietti, *Angew. Chem. Int. Ed.* **2012**, *51*, 68; *Angew. Chem.* **2012**, *124*, 70; d) R. S. Sprick, J.-X. Jiang, B. Bonillo, S. Ren, T. Ratvijitvech, P. Guiglion, M. A. Zwijnenburg, D. J. Adams, A. I. Cooper, *J. Am. Chem. Soc.* **2015**, *137*, 3265–3270; e) Y. Zheng, L. Lin, B. Wang, X. Wang, *Angew. Chem. Int. Ed.* **2015**, *54*, 12868–12884; *Angew. Chem.* **2015**, *127*, 13060–13077; f) R. S. Sprick, B. Bonillo, R. Clowes, P. Guiglion, N. J. Brownbill, B. J. Slater, F. Blanc, M. A. Zwijnenburg, D. J. Adams, A. I. Cooper, *Angew. Chem. Int. Ed.* **2016**, *55*, 1792–1796; *Angew. Chem.* **2016**, *128*, 1824–1828.

[8] a) I. Ghosh, T. Ghosh, J. I. Bardagi, B. König, *Science* **2014**, *346*, 725–728; b) C. D. McTiernan, S. P. Pitre, J. C. Scaiano, *ACS Catal.* **2014**, *4*, 4034–4039.

[9] V. Coropceanu, J. Cornil, D. A. da Silva Filho, Y. Olivier, R. Silbey, J.-L. Brédas, *Chem. Rev.* **2007**, *107*, 926–952.

[10] J.-L. Bredas, *Mater. Horiz.* **2014**, *1*, 17–19.

[11] L. Furst, B. S. Matsuura, J. M. R. Narayanam, J. W. Tucker, C. R. J. Stephenson, *Org. Lett.* **2010**, *12*, 3104–3107.

[12] a) Z. J. Wang, S. Ghasimi, K. Landfester, K. A. I. Zhang, *Adv. Mater.* **2015**, *27*, 6265–6270; b) R. Li, Z. J. Wang, L. Wang, B. C. Ma, S. Ghasimi, H. Lu, K. Landfester, K. A. I. Zhang, *ACS Catal.* **2016**, *6*, 1113–1121.

[13] See Ref. [11].

[14] D. A. Nagib, D. W. C. MacMillan, *Nature* **2011**, *480*, 224–228.

[15] M. Belletete, L. Mazerolle, N. Desrosiers, M. Leclerc, G. Durocher, *Macromolecules* **1995**, *28*, 8587–8597.

Received: April 19, 2016
Published online: July 5, 2016

